

Simplified method to detect resonance effects in railway bridges. Viaduct over Aragón River and Almonte bridge application

Javier Sánchez-Haro^{a,b}, Begoña Fernández^{a,b,*}, Guillermo Capellán^b, Emilio Merino^b

^a Department of Structural Engineering, University of Cantabria, Av. de los Castros 44, Santander 39005, Spain

^b Arenas&Asociados Ingeniería de Diseño S.L., Marqués de la Ensenada 11, Santander 39009, Spain

ARTICLE INFO

Keywords:

Resonance velocity
Simplified method
Almonte bridge
Railway
Dynamic analysis
Dynamic influence line

ABSTRACT

Detecting resonant effects in bridges has been studied for many years, but it has only been solved in a closed form for simple bridges. This article presents a simplified method that enables the calculation of resonance velocities in all types of bridges in an easy manner. The method is based on the concept of dynamic influence line and is validated through finite element models. These models range from simply supported bridges to complex real bridges such as the Almonte Viaduct, the world's longest arch bridge of its typology. In the real bridge models, a dynamic analysis is performed according to the Eurocode to identify train velocities that induce resonant effects, and these velocities are checked against the simplified method with very good results.

1. Introduction

The main dynamic design standards for railway bridges are Eurocode [1] and Arema [2], as they are the reference standards for many local regulations [3,4]. Both regulations share similar philosophies, running different standard trains at different velocities within the design velocity range, with a marked step between velocities to be refined if a resonant effect is detected. All cases covered above must be studied at least twice. Once for the maximum bridge weight situation and once for the minimum bridge weight situation, as the bridge vibration modes are affected. Neither standard indicates how many sections and at which locations the accelerations resulting from the dynamic analyses need to be evaluated. This large number of cases, not without uncertainty, represents such a high computational cost that dynamic analyses are only carried out in the final phase of the bridge design when the geometry is already defined. Therefore, if the dynamic analysis reports inappropriate dynamic behaviour of the structure, it often causes major setbacks at the design level. To avoid this situation, known geometric solutions, which may not be optimal, tend to be used to avoid setbacks. Even when the dynamic analysis has been carried out, there is no simplified calculation method available to ensure that the results provided by the FE models are correct, since the use of these programs requires decisions to be made that can affect the dynamic results, for example, the discretisation used [5].

The simplified method presented in this article has been developed

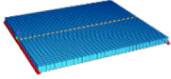
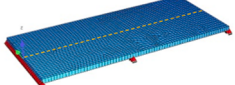
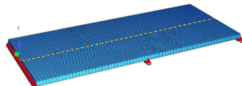
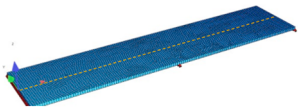
to; avoid the need for such a large number of cases, to be able to perform dynamic calculations at early stages of the project to provide more efficient solutions, to know which sections need to be evaluated in a dynamic calculation and to be able to check the results of an FE model. Analytical solutions to detect resonant effects have been developed over the years, but always for simply supported bridges [6–8]. Nowadays, there are fundamental theories and analytical methods for simple supported bridges [9], but the research into dynamic calculations continues, for example: the interaction of the structure with differential settlements [10], with the terrain [11], or with the vehicle [12–14]. The effect of vehicle-structure interaction has been implemented, for example, in the analytical solution to determine resonant effects, but in simply supported bridges with one span [15,16] or two spans [17,18], or one span with end restraints [19]. In more complex bridges, resonance calculations by simplified methods is performed either based on statistical analysis with the aim simply to detect trends [20] or by semi-empirical methods [21]. Moreover, there are methods based on the Fourier series [22] for continuous beams, but again, the mathematical complexity reduces their practical applicability. Additionally, there are interesting dynamic studies that relate bridge acceleration to train velocity to generate prevention alarms [23,24] and that measure vibration mode accuracy in real bridges detecting free vibration situations [25]. Some research studies are based on monitoring data to analyse dynamic behaviour of bridges, such as real damping ratios in bridges [26] or the damage level through neural networks [27].

* Corresponding author at: Department of Structural Engineering, University of Cantabria, Av. de los Castros 44, Santander 39005, Spain.

E-mail address: begoña.fernandezl@alumnos.unican.es (B. Fernández).

Table 1

Main analysis parameters and FE models for cases from C1 to C4.

Case	No of spans	Span Length (L)	Span Ratio	Vel. Range (km/h)	Damping (%)	Load Type	FE Model
C1	1	18	-	20-320	0.0	AA	
C2	2	18 + 18	1.00	20-400	0.0	AA	
C3	2	16 + 20	0.80	20-400	0.0	AA	
C4	2	$L^* + L^*$	1.00	289	0.0	AA	

* The span length L of the spans varies from 9 m to 63 m.

Finally, due to mathematical complexity or due to the limitations of the methods, only FE models are generally used to perform dynamic calculations in design bridge companies. However, they demand simple methods to check FE models. In that context, the proposed simplified method offers different novelties compared to the methods listed previously, that include: ease of use from a practical standpoint, resonance velocity detection even in complex bridges, identification of critical points of the bridges, and providing a useful tool to be applied both in the design phase stage and in the calculation stage, to check FE model results easily. For all these reasons, it is believed that the simplified method presented here can provide an easy and reliable tool for the contrast analysis of resonant effects with FE models in complex bridges, saving computational cost, incorporating design criteria in early phases of the bridge project and, ultimately, providing understanding of resonance more easily in all types of structures under the passage of moving loads. This article is structured in an Introduction that contextualises the problem and discusses the lack of knowledge on this subject in the main bridge design regulations. Next, a description is provided of the cases analysed and the computer tools (finite element models, FEMs) with which the analysis was carried out in the Materials and Methods section. The “Basis of Simplified Method” section describes the proposed formulation and verifies it for simple ideal bridges. Then, in the section “Validation of Simplified Method”, two results from two real bridges with real FE design models are compared with results from the proposed simplified method. Finally, the main conclusions of the research are presented.

2. Materials and methods

A total of 6 dynamic analyses were carried out on 6 different

structures, divided into 4 case studies on idealised bridges and 2 application cases on real High-Speed Railway bridges. In all of them, the performance of the proposed simplified method is analysed. The 4 case studies were modelled with the finite element program Sofistik with plate type elements. Sofistik is a calculation program that is well known for static [28] and dynamic modelling of bridges [29,30]. The 2 application cases were modelled using beam elements with the FE program Midas Civil, which is also extensively used in modelling static [31] and dynamic behaviour of bridges [32,33]. FE models of the application cases were provided by the company Arenas&Asociados for this research, which was therefore carried out with the real calculation models with which these bridges were designed. Thus, different types of models (slab and beam models) and different finite element software packages (Sofistik and Midas) were used in order to demonstrate that simplified methods provide reliable results in all cases.

2.1. Case studies

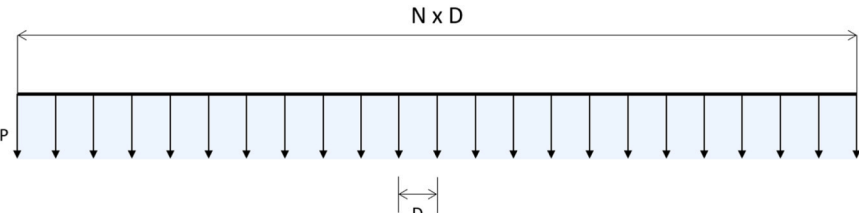
For the 4 case studies, simply supported slab bridges with a width of 15.56 m and a constant depth of 0.8 m of solid section were considered. The first 3 cases (C1 to C3) have a modulus of elasticity similar to that of concrete ($3.5\text{e}7 \text{ kN/m}^2$), while the fourth (C4) has a variable modulus of elasticity, in order to keep the vibration frequency constant when varying the geometry. The specific weight for cases C1 to C4 is similar to that of concrete (25 kN/m^3). The main parameters of the dynamic analyses and the FE models of each structure are shown in Table 1. For the study of the resonance phenomenon in cases C1 to C4, the two main bending modes of each structure were analysed.

For the case studies C1 to C4, the load sequence from the considered train is as defined in Table 2. The train travels at a constant velocity

Table 2

Load sequence from AA train for case studies C1 to C4.

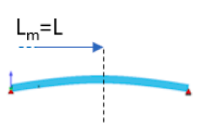
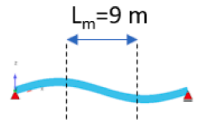
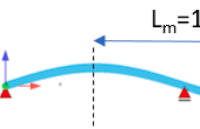
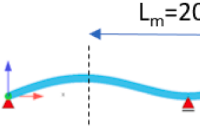
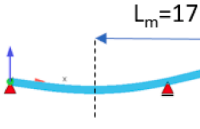
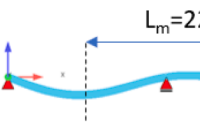
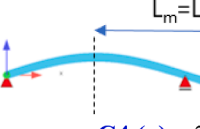
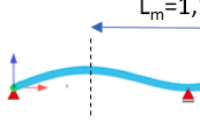
Train	Number of axles N	Distance between axles D (m)	Point forces P (kN)
AA	23	18	170

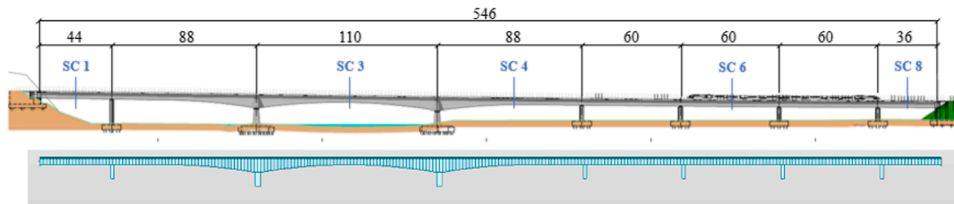


The diagram illustrates the load sequence for the AA train. It shows a horizontal line representing the bridge deck. Above the line, a long double-headed arrow is labeled $N \times D$, indicating the total length of the train. Below the line, 23 vertical arrows pointing downwards represent the point forces P . The distance between the first and second force is labeled D .

Table 3

Modes of vibration 1 (a) and 2 (b) in load cases C1 to C4.

Case	Modes of vibration	
C1	 C1 (a) – 2.86 Hz	 C1 (b) – 11.40 Hz
C2	 C2 (a) – 2.86 Hz	 C2 (b) – 4.46 Hz
C3	 C3 (a) – 2.68 Hz	 C3 (b) – 4.86 Hz
C4	 C4 (a) – 2.86 Hz	 C4 (b) – 4.46 Hz

**Fig. 1.** Geometric definition (above) and FE model (below) of the Viaduct over the Aragón River (C5).

along the longitudinal axis of the structure. All the case studies were analysed with a damping of 0%. The modes of vibration considered in cases C1 to C4, as well as the distance between points of maximum displacement (L_m), are shown in Table 3.

2.2. Application cases

The method proposed in this article was applied to two real High-Speed concrete bridges. Two bridges of different typology were chosen, one is a variable span girder bridge and the other is an arch bridge, since this typology, due to its uniqueness, is a focus of interest for dynamic study [34,35]. The bridges are shown below:

- Viaduct over the Aragón River (C5), part of the Cantabrian-Mediterranean corridor High-Speed line, near the town of Marcilla, Spain, Fig. 1, Fig. 2.
- Almonte Viaduct (C6), part of the Madrid-Extremadura corridor High-Speed line, at the Alcántara reservoir, Spain, Fig. 3, Fig. 4.

World record in its typology [36–41], concrete arch bridge for railways, 384 m main span.

The moving loads applied to both bridges correspond to the trains defined in the Eurocode [1]. Their definition is shown below, Fig. 5.

For the Viaduct over the Aragón River (C5), the first 20 modes of vibration of the structure were analysed in the "empty" state, that is, considering the self-weight and the permanent load. The first 20 vibration frequencies are shown in Table 4:

In the dynamic analysis carried out on the Almonte Viaduct (C6), the first 100 modes of vibration of the structure in the "empty" state were analysed, considering the self-weight and the permanent load. The first 100 vibration frequencies are shown in Table 5:

The summary of the characteristics of the dynamic analyses performed in Cases C5 and C6 are shown in Table 6:

3. Basis of simplified method

The proposed simplified method for detecting resonance effects in

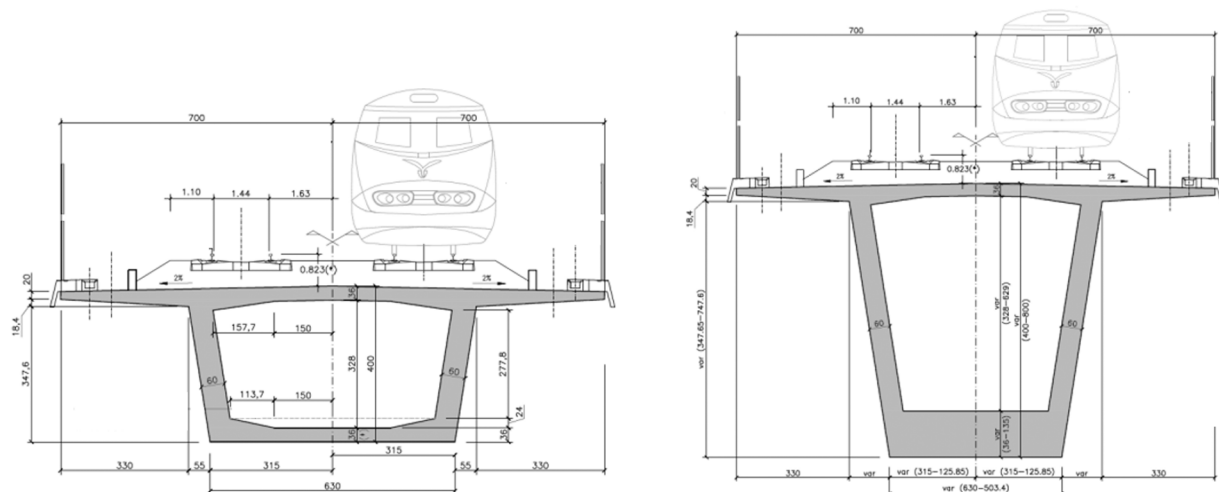


Fig. 2. Deck cross-section for constant depth (left), variable depth (right), Viaduct over the Aragón River (C5).

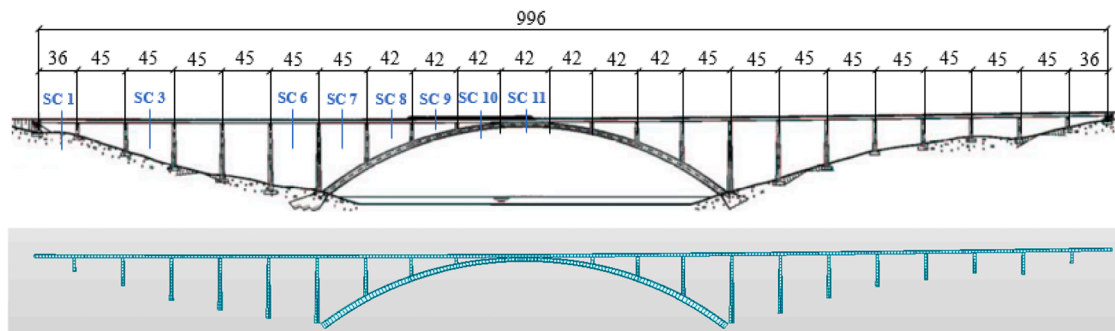


Fig. 3. Geometric definition (above) and finite element model (below) of the Almonte Viaduct (C6).

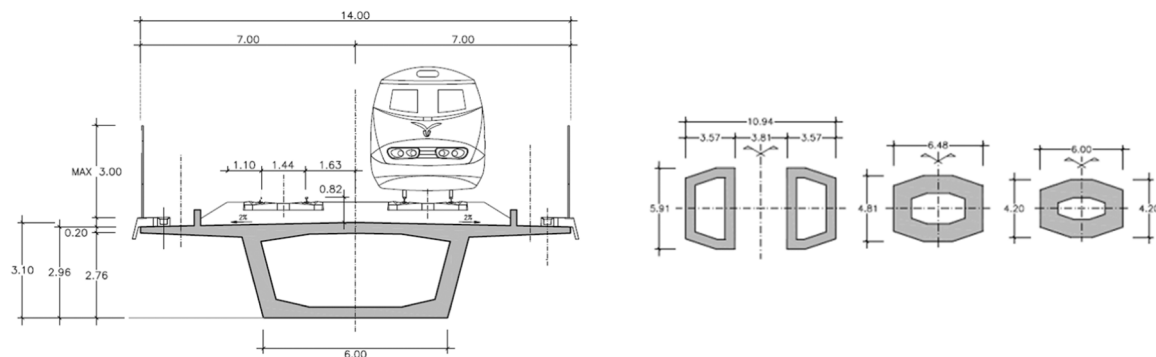


Fig. 4. Typ. Deck cross-section (left) and arch cross-sections (right), Almonte Viaduct (C6).

railway bridges and its theoretical basis is developed and explained below. Firstly, the concept of the dynamic influence line is deduced. Secondly, the expression for the resonance velocity is obtained. Subsequently, the influence of the equivalent force and the influence of the relative span length are analysed. Additionally, since the previous case analyses focused solely on flexural modes of vibration, the simplified method has been applied to include a torsional mode of vibration to comprehensive the research. Finally, based on all the above, the methodology of the simplified method is presented.

3.1. Dynamic influence line

In this section, the concept of dynamic influence line is developed as

the theoretical basis of the simplified method presented in this research. In other words, this section demonstrates how, when a dynamic load is located at one point of a structure, the equivalent load acting on another point of that structure can be estimated from the mode of vibration. That is, how the deformation of a mode of vibration can be associated with a line of influence when the loads are dynamic. To approximate the problem, we will first consider how to calculate the effective part of a load in a static analysis. In a simply supported beam under a distributed load $q(x)$, Fig. 6a, we want to know which equivalent force $F_{eq}(L/2)$ located at the centre of the beam, Fig. 6b, produces the same displacement at the centre of the beam $d(L/2)$ as the load $q(x)$.

If the equivalent force, but of opposite sign, Fig. 6c, were added to the original situation of the distributed load, Fig. 6a, the result at the

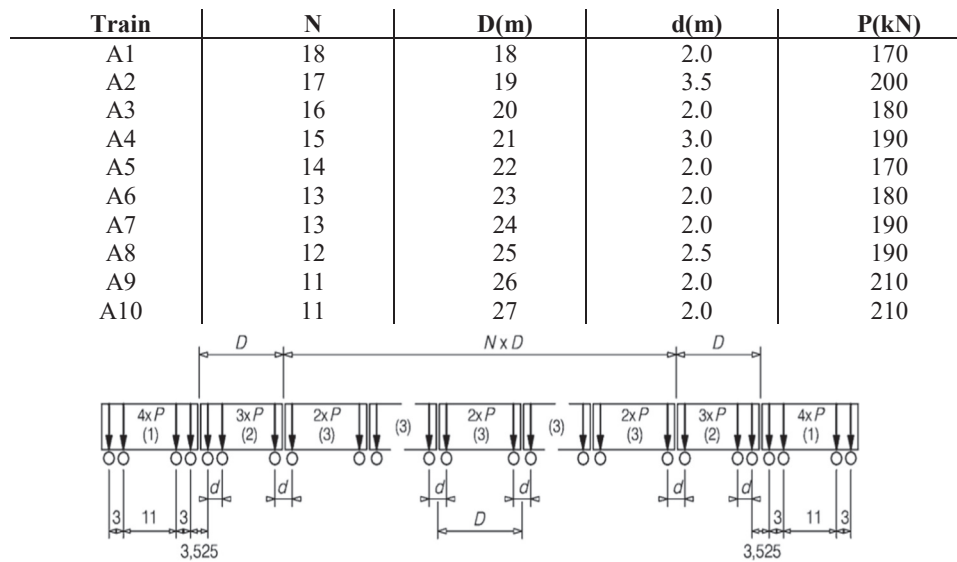


Fig. 5. Train loads (A1-A10) from Eurocode.

Table 4
First 20 natural frequencies of Aragón Viaduct.

Mode	f (Hz)	Mode	f (Hz)	Mode	f (Hz)	Mode	f (Hz)
1	0.94	6	2.30	11	3.69	16	4.70
2	1.33	7	2.50	12	3.92	17	4.79
3	1.58	8	2.74	13	4.01	18	5.33
4	1.61	9	2.87	14	4.04	19	5.91
5	2.09	10	3.50	15	4.07	20	6.00

point of application of the equivalent force would be a zero displacement, as if it were a support. In other words, the equivalent force that produces the same displacement as any force system at a point can be calculated as the reaction that occurs at an "imaginary" support placed at that point, Fig. 6d. Once the static case has been explained, the dynamic case is analysed. Everything explained in the static case is applicable in the dynamic case, the only difference being that in the dynamic case the reaction of the imaginary support varies with time. To analyse this variation, this article proposes the modification of Maxwell's theorem to consider it in a dynamic analysis. We start from the previous beam with the imaginary support at the centre of the beam. Consider for this

situation two independent states. First, the state (0), Fig. 7a, where a unit dynamic load is located at point x , is applied at instant t and produces a displacement under it of value $d_{(x,t)}^{(0)}$. Secondly, state (1), Fig. 7b, where a unitary abrupt displacement of the imaginary support has occurred which causes the deformation vibration mode $d_{(x,t)}^{(1)}$ to be activated.

$$W_{ext}^{(1)} = F_{eq(L/2,t)}^{(1)} 1$$

Table 6
Summary of load Cases C5 and C6.

N°	Bridge Length	N° of modes	Load type	Vel. Analised (km/h)	Vel. Step (km/h)	Damping (%)
5	546 m	20	A1-A10	20-410	10	0
6	996 m	100	A1-A10	20-420	10	5

Table 5
First 100 natural frequencies of Almonte Viaduct.

Mode	f (Hz)	Mode	f (Hz)	Mode	f (Hz)	Mode	f (Hz)	Mode	f (Hz)
1	0.27	21	2.48	41	4.02	61	7.34	81	9.19
2	0.56	22	2.56	42	4.07	62	7.56	82	9.24
3	0.75	23	2.67	43	4.25	63	7.64	83	9.36
4	0.79	24	2.73	44	4.25	64	7.67	84	9.57
5	0.89	25	2.78	45	4.39	65	7.82	85	9.94
6	0.89	26	2.88	46	4.49	66	7.90	86	9.95
7	0.94	27	2.971	47	4.57	67	8.00	87	10.20
8	1.10	28	3.07	48	4.57	68	8.12	88	10.28
9	1.21	29	3.17	49	4.59	69	8.28	89	10.92
10	1.23	30	3.24	50	4.67	70	8.31	90	11.45
11	1.41	31	3.27	51	4.71	71	8.40	91	11.53
12	1.42	32	3.56	52	4.82	72	8.46	92	11.94
13	1.45	33	3.57	53	5.16	73	8.49	93	12.04
14	1.48	34	3.58	54	5.33	74	8.57	94	12.25
15	1.69	35	3.59	55	5.43	75	8.63	95	12.44
16	1.79	36	3.75	56	5.58	76	8.71	96	12.63
17	1.96	37	3.79	57	5.76	77	8.91	97	12.86
18	2.23	38	3.84	58	6.24	78	8.91	98	12.89
19	2.36	39	3.97	59	6.53	79	9.05	99	12.99
20	2.40	40	3.97	60	7.01	80	9.18	100	13.20

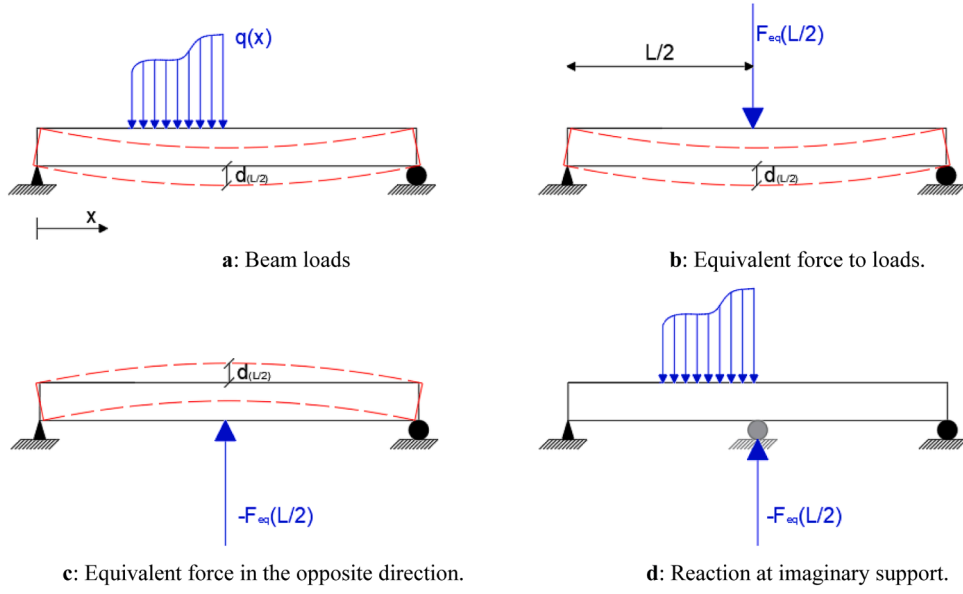


Fig. 6. a: Beam loads,; Equivalent force to loads: Equivalent force in the opposite direction.: Reaction at imaginary support.

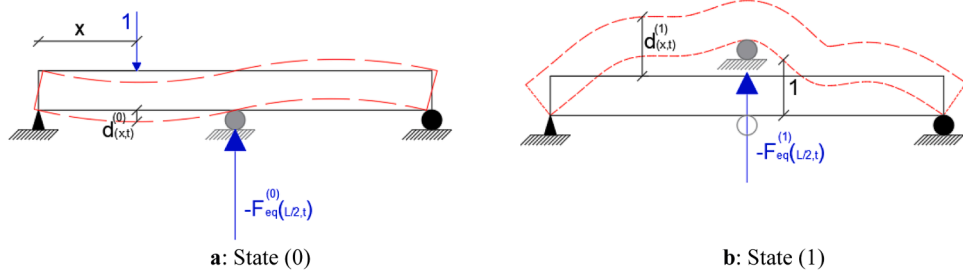


Fig. 7. a: State (0): State (1).

If we analyse the work of the external forces done in a third state, state (2), the sum of state (0) at first and state (1) afterwards, the result would be:

$$W_{ext}^{(0+1)} = 1d_{(x,t)}^{(0)} + F_{eq(L/2,t)}^{(1)} 1 - 1d_{(x,t)}^{(1)} + F_{eq(x,t)}^{(0)} 1$$

If we calculate state (2) as the sum of state (1) in the first place plus

state (0) we obtain:

$$W_{ext}^{(1+0)} = F_{eq(L/2,t)}^{(1)} 1 + 1d_{(x,t)}^{(0)}$$

Assuming linear behaviour of the structure, state (2) must be equal regardless of the loading process, therefore:

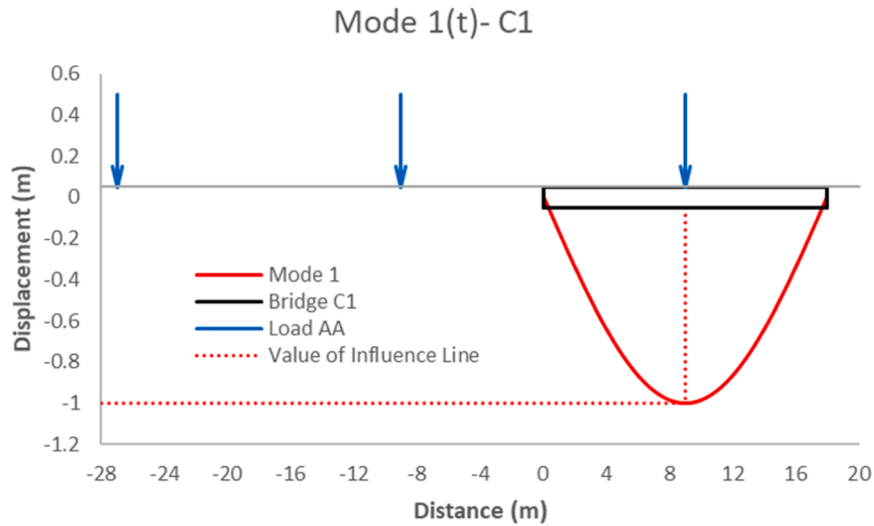


Fig. 8. Vibration mode 1 of case C1 at instant t .

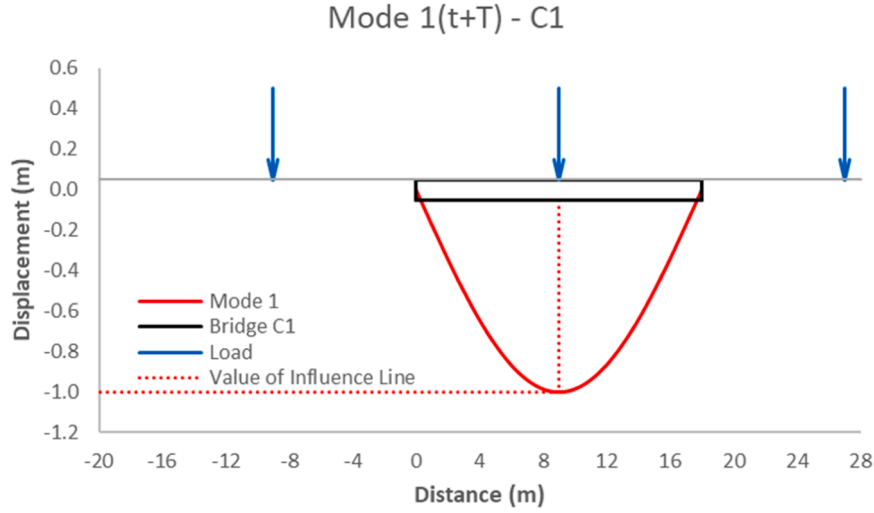


Fig. 9. Vibration mode 1 of case C1 at instant $t + T$.

$$W_{ext}^{(0+1)} = W_{ext}^{(1+0)}$$

$$F_{eq(L/2,t)}^{(0)} = d_{(x,t)}^{(1)}$$

That is, the reaction of the imaginary support and, therefore, the equivalent force when a load acts at a position x of the structure at instant t , is the deflection in state (1), at that point x and instant t . Where $d_{(x,t)}^{(1)}$ is the dynamic and deformed influence line of any given mode of vibration for instant t . In principle, the line of influence for another instant would be different, since the amplitude of the mode of vibration oscillates with time. However, if the loads are applied at instant $t + nT$, where n is a natural number and T is the period of vibration, then the dynamic influence line remains constant because the amplitude of the mode of vibration is constant for multiples of the period.

3.2. Resonance velocity

In this section, a general expression for resonance velocity is deduced. In order to clarify it with an example and to demonstrate it numerically, this section uses a FE model to analyse the single-span bridge of case C1, whose mode 1 has a frequency f of value 2.86 Hz. The load sequence from AA train has a wheelbase of $D = 18$ m, see Table 1. Considering the previous section, mode of vibration 1 corresponds to the line of influence of the equivalent force at the centre of the span, Fig. 8. The loads of the AA train are positioned on the dynamic line of influence (maximum unit amplitude) so that the equivalent force is maximum, for a given instant t . Therefore, a load is placed in the centre of the span, leaving the rest of the loads outside the structure due to the geometry of the bridge and the load sequence from AA train, as shown in Fig. 8. In this configuration, as a consequence of the geometry of the line of influence, the load is most effective when it is in the centre, that is, $F_{eq} = 1P = P$. If, due to the forward velocity of the train AA, the second load is at the same position as the first load was when the mode of vibration is at the same position at instant t , the equivalent force on the structure will be added to the previous one $F_{eq} = 1P + 1P = 2P$, Fig. 9.

The fact that the line of influence is at the same position at instant t when the second load passes through the centre of the span ($t + T$), defines the velocity V of movement of the loads, since the time between two equal positions of the mode is precisely the period T . As the distance between loads is constant, D , this process will be repeated for all the loads if the velocity V also remains constant, being in that case $F_{eq,end} = mP$ where m is the number of loads and, therefore, a resonance process will occur in the bridge because with each transit of load the F_{eq} will increase. The velocity associated with this process will be the resonance

Table 7

Considered resonance velocities for case C1 calculated with Eq. (1).

	D	f	n	V (km/h)
$V_{r,m1,n=1}$	18	2.86	1	185.3
$V_{r,m1,n=2}$	18	2.86	2	95.7
$V_{r,m1,n=3}$	18	2.86	3	61.8
$V_{r,m2,n=1}$	18	11.40	1	738.7

velocity $V_{r,mi,n=1}$ of that mode of vibration i for a time separation between loads nT , with $n = 1$, and it can be calculated as the distance between loads D divided by the period of vibration T associated with the frequency of the mode f . Thus, the resonance velocity results in Eq. (1):

$$V_{r,m,n} = \frac{D}{nT} = \frac{Df}{n} \quad (1)$$

For case C1, the resonance velocities are shown in Table 7:

The point of the structure with maximum acceleration associated with this resonance velocity will be the centre of the span, because it is the point of maximum displacement of the mode that is activated, mode 1. In Fig. 10, the maximum acceleration of the span centre on transit of the load sequence from AA train is shown for the different velocities evaluated based on FE model results. The resonance velocity $V_{r,m1,n=1}$ from Table 7 marked with a vertical line for the value of 185.3 km/h matches perfectly with the peak of maximum accelerations shown by the diagram obtained.

In other words, the resonance velocity of the bridge in case 1 was predicted correctly.

In addition, minor peaks can be found in Fig. 10 around the velocities of approximately 90 and 60 km/h. The explanation for these acceleration peaks associated with those velocities is as follows. From what has been stated so far, it has been assumed that the loads take a time equal to the vibration period T to reach the position of the predecessor, but in reality, they could take a time multiple of nT ($n = 2, n = 3$, etc.) and the amplitude of the mode position, or line of influence, would remain the same when the load passes through the centre of the span. In this way, we can speak of resonance velocity submultiples, and they are calculated in Table 7 ($V_{r,m1,n=2}$ and $V_{r,m1,n=3}$). As can be seen in Fig. 10, the resonance velocities for $n = 2$ and $n = 3$, marked with a vertical line, match perfectly with the small acceleration peaks. Note that the values presented in Table 7 match the values obtained with the method outlined in [21]. The accelerations associated with sub-multiple velocities are always much smaller than the acceleration for $n = 1$ because they occur for lower velocities and, furthermore, because they are influenced by

ACCELERATION Vs VELOCITY - CASE C1

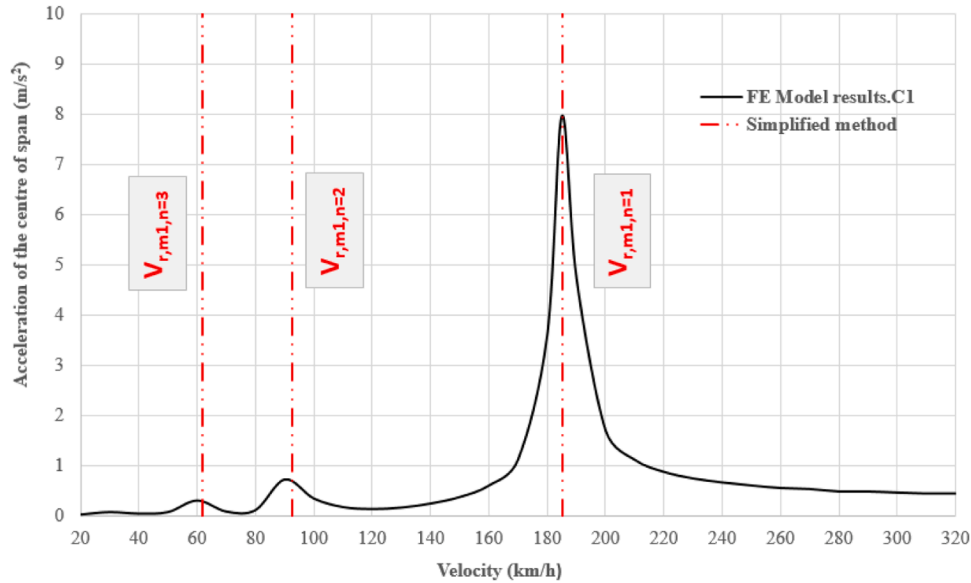


Fig. 10. Diagram of maximum span centre accelerations of case C1. FE Model Vs Simplified method.

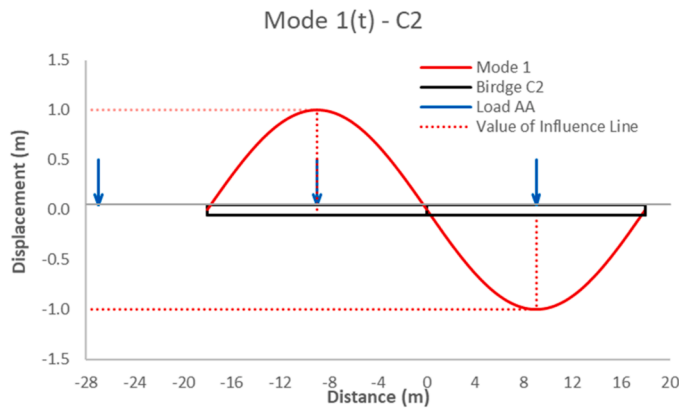


Fig. 11. Vibration mode 1 in case C2 at instant t .

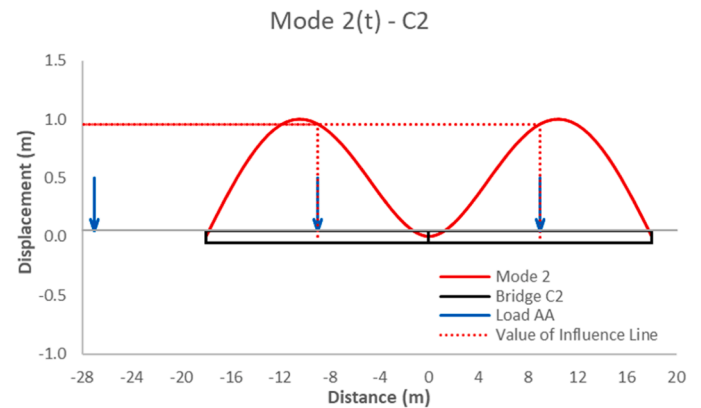


Fig. 12. Vibration mode 2 in case C2 at instant t .

damping. As the structure vibrates freely for a time equal to several periods before the arrival of the next load, the damping dissipates the energy of the system before reintroducing energy. Moreover, submultiples in complex structures do not always produce acceleration peaks, as the process of load arrival up to the point of maximum equivalent load can have its influence and virtually eliminate the acceleration peak associated with a submultiple velocity. In the same way that the resonance velocity of mode 1 was calculated, the resonance velocity of mode 2 can be obtained for $n = 1$ in case C1. For this mode, the resonance velocity would be:

$$V_{r,m2,n=1} = \frac{D}{T} = Df = 18 \times 11.40 \times 3.6 = 738.7 \text{ km/h}$$

This velocity is outside the range of velocities studied in case C1, so it should not be considered. In any case, if the velocity range were up to 800 km/h, due to the shape of this second mode, this velocity would not trigger mode 2 for the reasons explained in the following section.

3.3. Influence of equivalent force

In this chapter, the influence of the equivalent force on resonant effects of the bridge is shown. To this end, a continuous structure with

two spans is analysed. Two cases will be shown, in the first one the length of the spans will be equal (C2) and in the second one they will have a ratio between them of 0.8 (C3). In both cases, results from Eq. (1) are compared with results from FE models.

3.3.1. Equal span lengths $L1/L2 = 1$

The simplified method is applied for case C2 in the same way as for case C1. First, vibration mode 1, which has a frequency of 2.86 Hz, is analysed. This mode is the line of influence of the equivalent force at either of the two span centres, as they have equal amplitude, Fig. 6a. Using the mode as the line of influence, the load sequence from AA train is placed so that it provides the maximum equivalent force. In this case, we place the first two loads of the AA train at the centre of the spans, Fig. 11.

In this case, the resonance velocity of mode 1 would be:

$$V_{r,m1,n=1} = Df = 18 \times 2.86 \times 3.6 = 185.3 \text{ km/h}$$

However, the equivalent force would be zero in this case, since, having amplitudes of opposite sign, the load of one span cancels out that of the other.

$$F_{eq} = 1P - 1P = 0$$

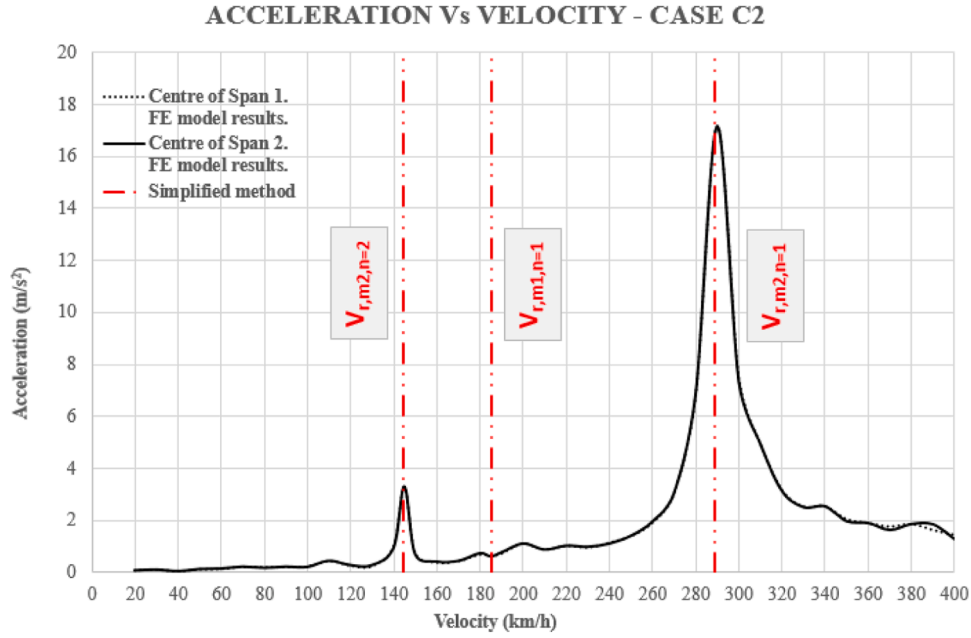


Fig. 13. Maximum acceleration diagram of the span centres. FE Model Vs Simplified method.

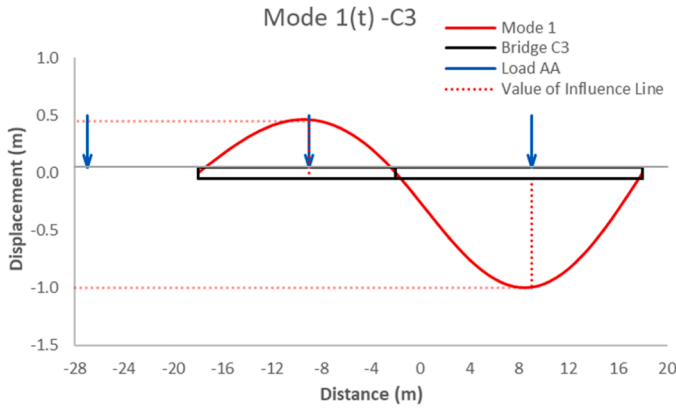


Fig. 14. Vibration mode 1 of case C2 at instant t .

Since this will happen with the following two loads of the AA train on the structure at instant $t + T$, the final equivalent force in this case is zero and therefore mode 1 will not be activated for its resonance velocity. The second mode is analysed next, placing the loads in the same way as for mode 1, Fig. 12, at instant t .

The resonance velocity in this case for the second mode is:

$$V_{r,m2,n=1} = Df = 18 \times 4.46 \times 3.6 = 289.0 \text{ km/h}$$

And the equivalent force for instant t will be:

$$F_{eq} = 0.95P + 0.95P = 1.8P$$

For instant $t + T$, mode 2 will have the same amplitude and, therefore, the equivalent force will increase with each step of the loads. Fig. 13 shows the result of the dynamic analysis of case C2. It shows the maximum acceleration of the centres of span 1 and span 2 (superimposed) in case C2 on transit of the load sequence from AA train for different velocities. It can be seen that for the value of the mode 1 resonance velocity ($V_{r,m1,n=1} = 185.3 \text{ km/h}$) marked with a vertical line, there is no acceleration peak. That is, the zero equivalent force prevents any resonant amplification from occurring. Note that according to the method outlined [21], there should be resonant effects for that velocity, but as can be verified with the finite element results (Fig. 13), there are

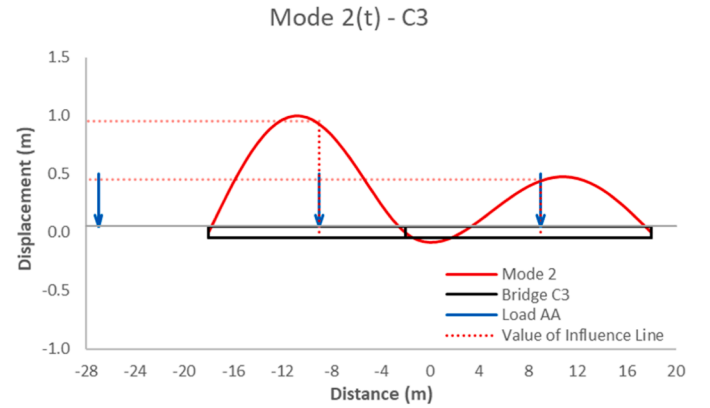


Fig. 15. Vibration mode 2 in case C3 at instant t .

none. The reason is that the simplified method showed in that research does not take into account the influence of the equivalent force. However, for the mode 2 resonance velocity value ($V_{r,m2,n=1} = 289.0 \text{ km/h}$), a very sharp peak appears.

Note that for a velocity value slightly above 140 km/h another minor peak appears. This peak corresponds to the submultiple of $V_{r,m2}$ for $n = 2$:

$$V_{r,m2,n=2} = \frac{Df}{2} = \frac{18}{2} \times 4.46 \times 3.6 = 144.5 \text{ km/h}$$

3.3.2. Unequal span lengths $L2/L1 = 1.25$

In this section, the case C2 process is repeated, but with unequal spans of ratio 0.80, case C3. Unlike what happened in case C2 for mode 1, because the spans are not exactly equal, when positioning the load sequence from AA train on mode 1, the equivalent force does not completely cancel out, Fig. 14.

The equivalent force, in absolute value, resulting from positioning the loads in this case is:

$$F_{eq} = +0.95P - 0.45P = 0.5P$$

The resonance velocity for mode 1 in this case is:

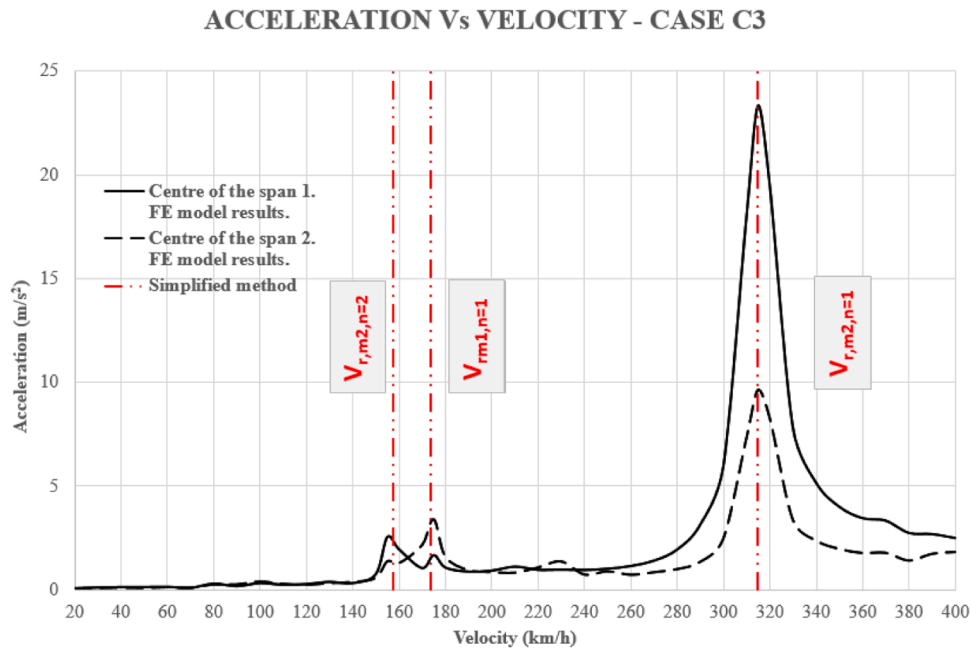


Fig. 16. Diagram of maximum span centre accelerations in case C3. FE Model Vs Simplified method.

$$V_{r,m1,n=1} = Df = 18 \times 2.679 \times 3.6 = 173.5 \text{ km/h}$$

As for the second mode, based on Fig. 15, the equivalent force and resonance velocity are:

$$F_{eq} = 1.0P + 0.4P = 1.4P$$

$$V_{r,m2,n=1} = Df = 18 \times 4.86 \times 3.6 = 314.9 \text{ km/h}$$

Fig. 16 shows the result of the dynamic analysis for case C3. It shows the maximum accelerations of the span centres on passage of the AA train for different velocities.

Fig. 16 shows that, unlike case C2, for the value of the resonance velocity of mode 1 ($V_{r,m1,n=1} = 173.5 \text{ km/h}$) marked with a vertical line, there is a small acceleration peak because the equivalent force is not zero, although it is small. For this velocity, it can be seen in Fig. 16 that the centre of span with the highest acceleration is the centre of span 2,

consistent with the deformation of vibration mode 1, Fig. 14. The large acceleration peak, as expected from the equivalent force, is for the resonance velocity of mode 2 ($V_{r,m2,n=1} = 314.9 \text{ km/h}$). In this case, because the activated mode is mode 2, it is span 1 that has the highest acceleration, consistent with the deformation of vibration mode 2, Fig. 15. Note that the ratio between the maximum accelerations of the two span centres is the same as the ratio between the displacements of the span centres of mode 2. In addition to the velocity associated with mode 1 and the velocity associated with mode 2, there is also a peak in the value of the submultiple of mode 2 and, therefore, with more acceleration at the centre of span 1:

$$V_{r,m2,n=2} = \frac{Df}{2} = \frac{18}{2} \times 4.86 \times 3.6 = 157.5 \text{ km/h}$$

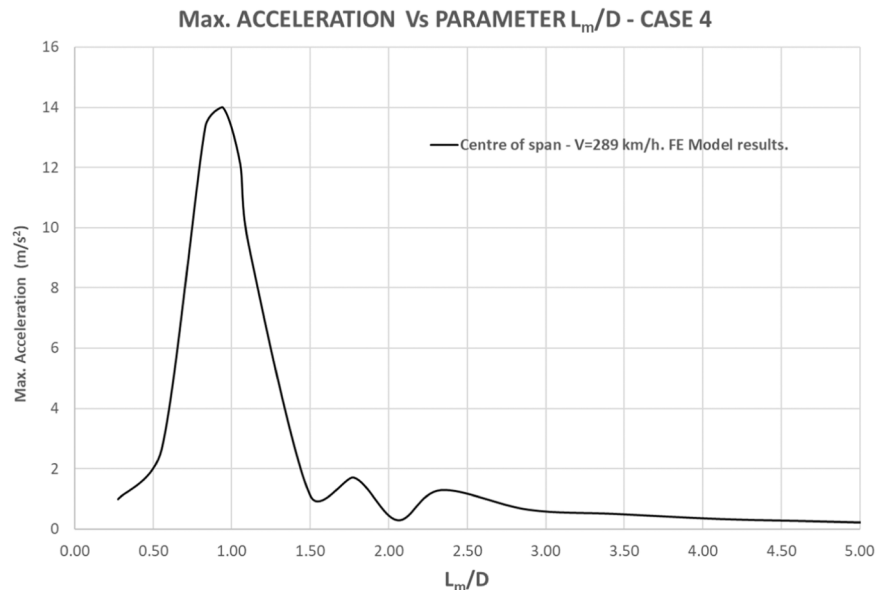


Fig. 17. Max. acc. Vs L_m/D parameter, case C4. Resonance vel. of mode 2 (289 km/h). FE Model results.

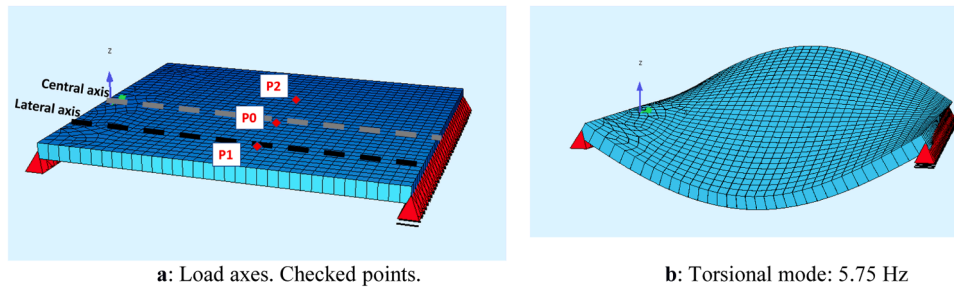


Fig. 18. a: Load axes. Checked points.: Torsional mode: 5.75 Hz.

3.4. Influence of the relative span length

The analysed cases shown so far (C1, C2 and C3) have in common that the distance between axes D is practically the same as the distance between the points of maximum displacements of the modes, parameter L_m , Table 3. This section analyses the influence of the relative span length in the resonance effects based on the L_m/D parameter. For this purpose, the dynamic analysis based on results from FE model in case C4 was carried out varying the parameter L_m/D between values of 0.5 and 5. The analysed bridge has two equal span lengths, but that length is changed in order to modify the parameter L_m/D while the modulus of elasticity is transformed in an appropriate way to balance the stiffness and keep the natural frequency constant. The velocity considered for the AA train to pass through structure C4 is 289.0 km/h for all values of the L_m/D parameter. This is the resonance velocity of mode 2 (mode 1 would not be activated for its resonance velocity because the displacement amplitude is equal in both spans, but of opposite sign). The results of the dynamic analysis in case C4 are shown in Fig. 17, where you can see the maximum acceleration of the centre of one span (the other span centre will have the same value due to the symmetry of the mode) as a function of the parameter L_m/D for the mode 2 resonance velocity.

As can be seen in Fig. 17, when the parameter L_m/D approaches 1, the acceleration value increases exponentially. Departing from that value, except for some small undulations in the environment between $L_m/D = 1.5$ and $L_m/D = 2.5$, the acceleration decreases very quickly. That is, for resonance to occur in a bridge when a train passes, there is not only a temporal factor (resonance velocity), but also a spatial factor (parameter L_m/D). Both factors have to be present for resonance to occur in significant terms. The explanation of how a large value of spatial factor L_m/D can avoid resonance is as follows. If L_m/D is sufficiently large, the loads will have practically not moved their relative position in the span during the time of a half-period T . That is, although it is the resonance velocity and, therefore, the load occupies the position of its predecessor in a time T , the movement is negligible regarding the length of the span. In this way, since the load is in an almost fixed position, the influence line adds approximately the same value during a half-period (positive mode amplitude) as it subtracts in the next half-period (negative mode amplitude). In conclusion, as the load practically does not move, the equivalent force provided by the dynamic line of influence is zero over a period T .

3.5. Torsional mode of vibration

So far, the analysed vibration modes have corresponded to flexural modes, as they are often the most relevant. However, the proposed simplified method can be applied to any vibration mode. To verify this, in this section, the C1 case is recalculated, but with the loads moving along the bridge on a laterally shifted axis of 3.8 m from the central axis, as shown in Fig. 18a. For this dynamic analysis, in addition to the flexural modes indicated in Table 3, the torsional mode with a frequency of 5.75 Hz is considered, as shown in Fig. 18b. Another difference from the analysis conducted in Section 3.2 is that in that section, only the

Table 8

Considered resonance velocities for case C1 with lateral and central axis calculated with Eq. 1.

			Flexural mode (m=1)		Torsional mode (m=2)	
			f (Hz)	2.86	f (Hz)	5.75
Train	D(m)	n	V_r (Km/h)		n	V_r (Km/h)
AA	18	1	185,5		1	372,4
AA	18	2	92,8		2	186,2
AA	18	3	61,8		3	124,1

accelerations of point P0, the central point, were checked, while now the accelerations of points P1 and P2, lateral points, are also analysed (Fig. 18a).

The results of resonance velocities obtained by applying Eq. 1 of the simplified method for both flexural and torsional modes are presented in Table 8.

In Fig. 19, the results from finite element analysis for points P0 (dashed line and dot, central axis) and P1 (solid line, lateral axis) are shown. Vertical lines identify the resonance velocities as indicated in Table 8, with a dashed line and double dot for the flexural mode ($n = 1,2,3$) and a dotted line for the torsional mode ($n = 1,2,3$). As observed in Fig. 19, for the velocity of 372 km/h at point P1 on the lateral axis, there is a peak acceleration in FE results coinciding with the resonance velocity predicted by the simplified method for the torsional mode, which is not present in FE results for the central axis at point P0. Note also that at point P1, at the velocity of 185 km/h, the acceleration is amplified compared to the central axis at point P0. This occurs because the flexural resonance velocity ($n = 1$) coincides with the first submultiple of the torsional resonance velocity ($n = 2$), and both modes are superimposed.

To confirm that the peak accelerations at 372 km/h are indeed due to torsion, the first few seconds of the acceleration-time diagrams for points P1 and P2 are shown for resonance velocities of 185 km/h (Fig. 20a) and 372 km/h (Fig. 20b). As evident in the resonance velocity of 185 km/h, the accelerations of points P1 and P2 coincide, characteristic of a longitudinal flexural mode. Conversely, at the resonance velocity of 372 km/h, the accelerations of points P1 and P2 exhibit opposite accelerations, indicative of a torsional mode, as predicted by the simplified method.

3.6. Simplified method methodology

Based on all the information presented in Section 3, the methodology of the simplified method is established and summarized in the following points:

1. Place the loads (train) on the vibration mode (influence line) looking for the maximum equivalent force to identify the vibration modes that will have a non-negligible equivalent force result. A quantitative analysis is sufficient. The remaining modes will not be activated.

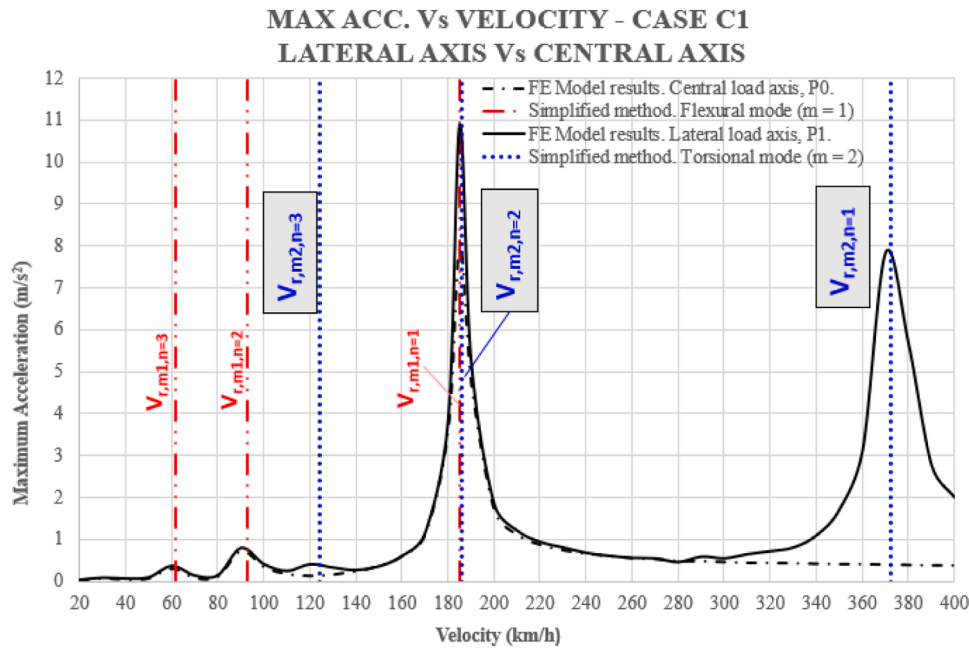
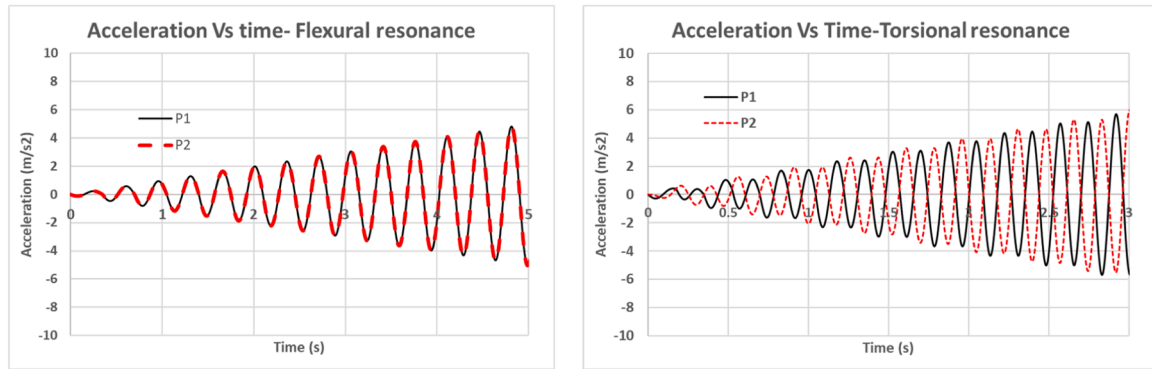


Fig. 19. Diagram of maximum accelerations at P1 of case C1. Lateral axis Vs Central axis. FE Model Vs Simplified method.



a: Accel. Vs Time diagram. Flexural resonance. $V=185$ km/h.

b: Accel. Vs Time diagram. Torsional resonance. $V=372$ km/h.

Fig. 20. a: Accel. Vs Time diagram. Flexural resonance. $V=185$ km/h. b: Accel. Vs Time diagram. Torsional resonance. $V=372$ km/h.

- From the selected modes of vibration, discard those where the maximum displacement occurs in a span with the parameter L_m/D greater than 2.0, as these modes will not be activated either.
- Calculate all resonance velocities for $n = 1$ according to Eq. 1 for all non-discarded vibration modes and for each train with different equispaced axle distances (although the locomotives and some wagons may not have equispaced axles, disregard their influence on the results and focus on the repeated axle pattern. The amplification due to repeated axles is much more significant than some loads that do not follow the pattern).
- If any of the resonance velocities for $n = 1$ for any vibration mode is outside the range of study velocities for that project, consider the resonance velocity of that mode for $n = 2$ according to Eq. (1) ($n \geq 3$ is considered negligible in any case).
- Each resonance velocity will present the maximum acceleration at the point of the bridge with the maximum displacement associated with the corresponding mode of vibration.

4. Validation of simplified method

In this section, the simplified method is validated using two real complex bridges: a deck arch bridge (Almonte Viaduct) and a continuous variable-depth box girder bridge (Viaduct over Aragón River). Both structures are analysed using a finite element (FE) model according to Eurocode verification methods, and the results are compared with those obtained using the simplified method.

4.1. Viaduct over Aragón River

Next, case C5 is analysed. This case is an analysis of a real bridge; the Viaduct over the Aragón River. The dynamic analysis was carried out according to Eurocode [1], the main characteristics of which are shown in Table 6. For this analysis, all span centres of different lengths have been checked, specifically the centres of spans 1, 3, 4, 6 and 8, Fig. 1. The simplified method explained in the article for detecting resonant effects for this real case has been applied. There are 20 vibration modes considered (Table 4), each of which will have a resonance velocity for each type of train, since they have different distances between axles.

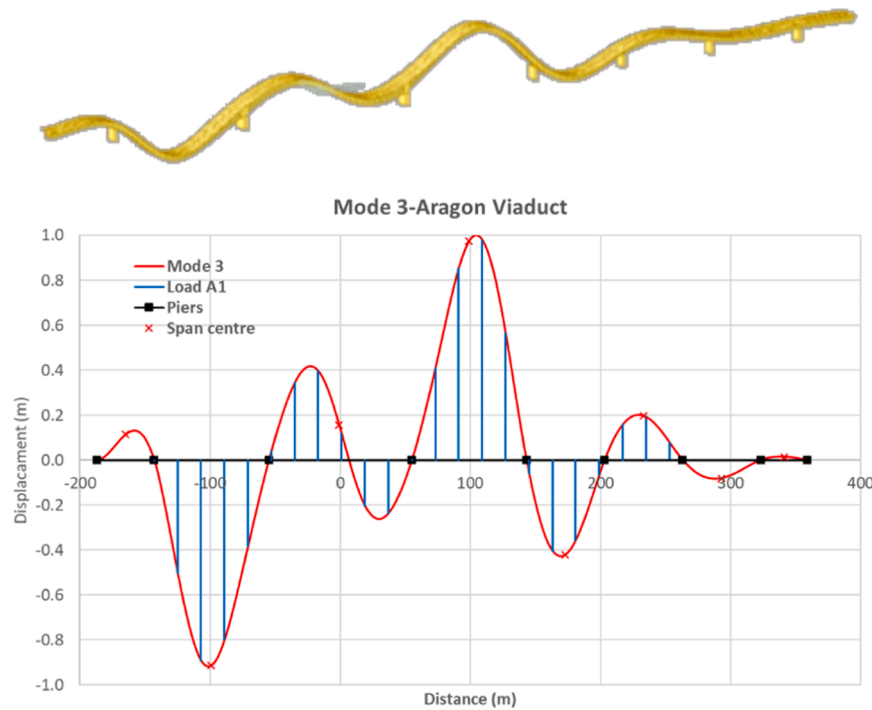


Fig. 21. Mode of vibration 3 of Viaduct over Aragón River. A1 train load placements.

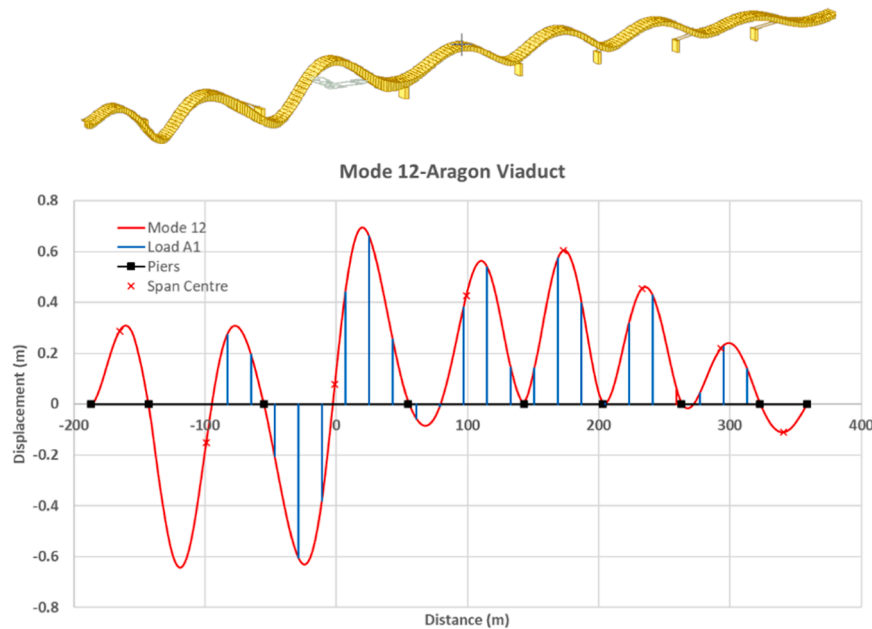


Fig. 22. Mode of vibration 12 of Viaduct over Aragón River. A1 train load placements.

Some resonance velocities will be above the 410 km/h project maximum velocity, so they will be beyond the study range. In that case, we would have to consider their largest submultiples within the study range. As there are 10 different trains and 20 modes of vibration, the total number of velocities that need to be checked is 200. Consequently, 20 check points along the bridge need to be considered per the maximum displacement in each mode of vibration. However, and after what was stated in the article, by analysing the shape of the vibration modes, the number of modes to be considered can be reduced. Specifically, the analysis of the modes of vibrations 3, 12 and 20 of the Viaduct over the Aragón River are shown in detail, as they are representative. Fig. 21

shows mode 3 with the placements of the loads of train A1. As can be seen, this mode will not be activated significantly. The equivalent force F_{eq} is very small because the loads cancel out, having the same values and opposite signs (check equal areas), just as happened in cases C2 and C3 for mode 1.

Fig. 22 shows the mode of vibration 12 with the placement of the train A1 loads. The shape of mode 12 does enable a non-negligible equivalent force (more and larger loads over the structure than under the structure). However, due to the length of the spans where the maximum displacement occurs, a value of $L_m/D \geq 2.2$ is produced for all trains A1-A10, so the activation of mode 12 will be residual. The

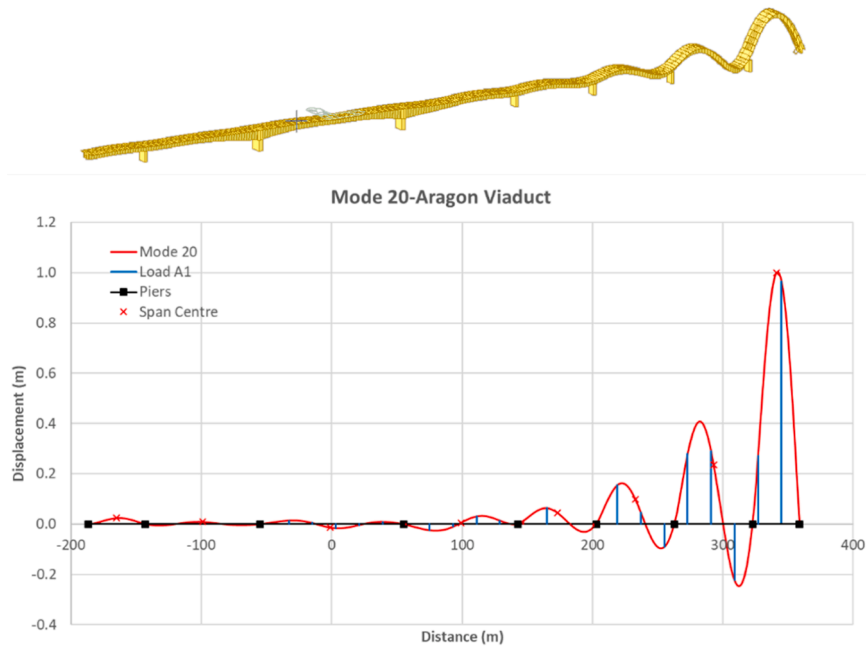


Fig. 23. Mode of vibration 20 of Viaduct over Aragón River. A1 train load placements.

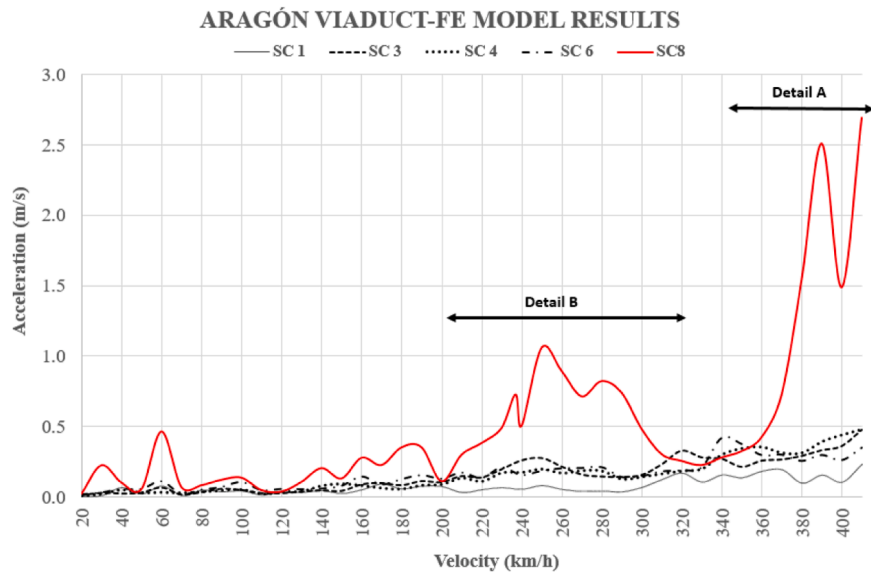


Fig. 24. Acc. envelope. Trains A1 to A10 in sections SC1, SC3, SC4, SC 6 and SC8. FE model results.

discussion of why modes 3 and 12 will not be activated (small F_{eq} and/or large L_m/D) are also applicable to the first 19 vibration modes of the Viaduct over the Aragón River.

Fig. 23 shows mode of vibration 20 with the placements of the train A1 loads. Mode 20 is the first mode that has a significant equivalent force result and L_m/D parameter values between 1.3 and 2, depending on the train considered. For this reason, it is the mode that will be activated with the highest intensity of the 20 modes of vibration considered in the analysis. Due to the fact that mode 20 presents the maximum displacement in the centre of span 8 approximately, it will be this section which develops the highest accelerations for the velocities corresponding with mode 20 frequency from train A1 to A10.

The results of the dynamic analysis of case C5 are shown in Fig. 24. Each line represents the envelope of the accelerations from trains A1 to A10 at the check sections defined in Fig. 1. As can be seen, the centre of span 8 (SC8) develops the highest acceleration peaks, consistent with the

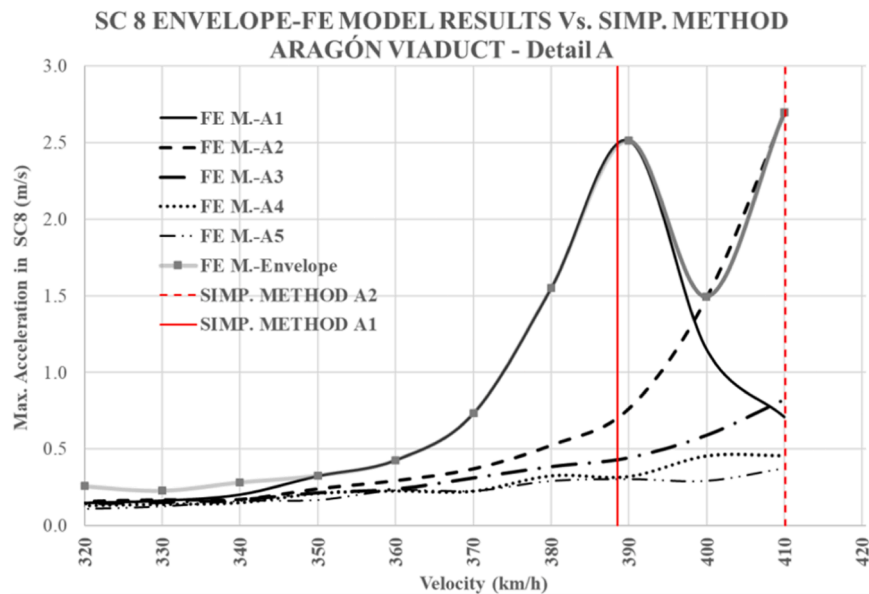
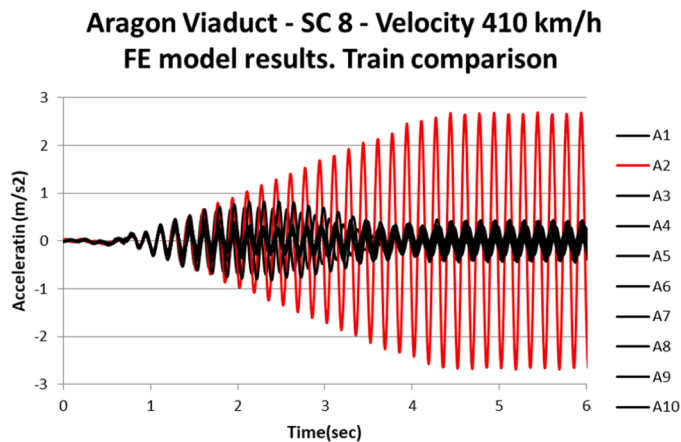
activation of mode 20. The check section SC8 has been studied deeply in the areas of greatest acceleration (detail A and detail B, Fig. 24) to check whether the acceleration peaks are caused by velocities predicted by the simplified method for each train.

The resonance velocities, $n = 1$, and the submultiple $n = 2$ for each train on mode of vibration 20 are shown in Table 9. Note that the values outside the project range (>410 km/h) are marked in grey.

The detail of zone A is shown in Fig. 25. In this figure, the law of maximum accelerations of each train (only trains from A1 to A5 are shown for the sake of clarity) forms the total envelope of section SC8 shown in Fig. 24 for velocities from 320 to 410 km/h. Note that above 350 km/h the envelope is formed by the resonance velocities of train A1 and A2. The resonance velocities of trains A1 and A2 shown in Table 9 have been highlighted with a vertical line. It can be seen that the acceleration peaks from dynamic analysis of the Aragón River Viaduct coincides perfectly with the resonance velocities shown in Table 9.

Table 9Resonance Velocities for $n = 1$ and $n = 2$ of mode 20 of Viaduct over Aragón River.

Mode 20	f (Hz) =5.996	$V_{r,m20,n}$ (km/h)	
Train	D (m)	n=1	n=2
A1	18	388.5	194.3
A2	19	410.1	205.1
A3	20	431.7	215.9
A4	21	453.3	226.6
A5	22	474.9	237.4
A6	23	496.5	248.2
A7	24	518.1	259.0
A8	25	539.6	269.8
A9	26	561.2	280.6
A10	27	582.2	291.4

**Fig. 25.** Analysis of Detail A. FE Model results Vs. Simpl. Method. Max acc. Vs Vel. of trains (A1-A5).**Fig. 26.** FE model results. Acceleration Vs time diagram at section SC8 of Aragón River Viaduct. Velocity 410 km/h. Trains A1 to A10.

To illustrate more clearly how resonance occurs only for a single train according to its specific resonance velocity, Fig. 26 shows the acceleration versus time diagram developed by section SC8 from the dynamic analysis of the Aragón Viaduct at a velocity of 410 km/h (resonance velocity of train A2 according to the results shown in Table 9).

It can be seen in Fig. 26 that train A2 (red line) produces an acceleration of 2.7 m/s^2 at section SC8 (as the envelope of Fig. 25 shows), while the rest of the trains (black lines) produce an acceleration under 0.8 m/s^2 . Detail B defined in Fig. 24 is shown in Fig. 27, where it is demonstrated that the envelope of each train (for clarity, only trains A5 to A10 are shown) forms the total envelope of section SC8 for the velocity range from 200 km/h to 350 km/h. The resonance velocities for $n = 2$ defined in Table 9 are highlighted with vertical lines. As can be seen in Fig. 27, the acceleration peaks coincide perfectly with the resonance velocities of the multiples of $n = 2$ for each train shown in Table 9. Under 190 km/h, it is the submultiples of $n > 2$ that generate the envelope, although with a non-zero damping these peaks would have been strongly reduced. For example, the peaks of 30 and 60 km/h shown in Fig. 24 are caused by train A8 with submultiples $n = 9$ and $n = 18$,

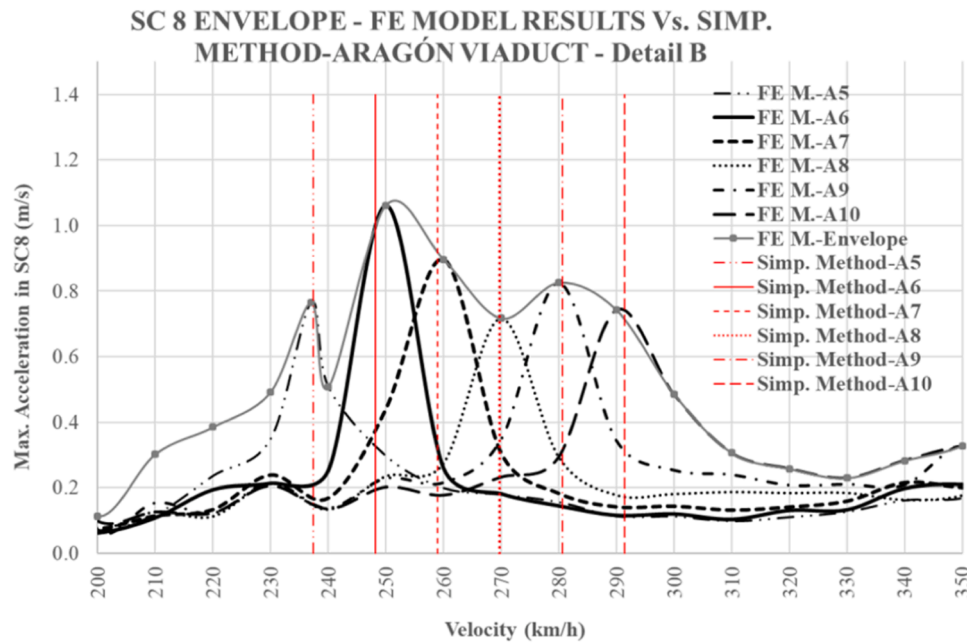


Fig. 27. Analysis of Detail B. FE model results Vs. Simp. Method Max. acc. Vs Vel. of trains (A5-A10). Note that the effect of the front and rear bogies does not modify the structural response, as their impact is negligible compared to the amplification caused by the repeated wagons.

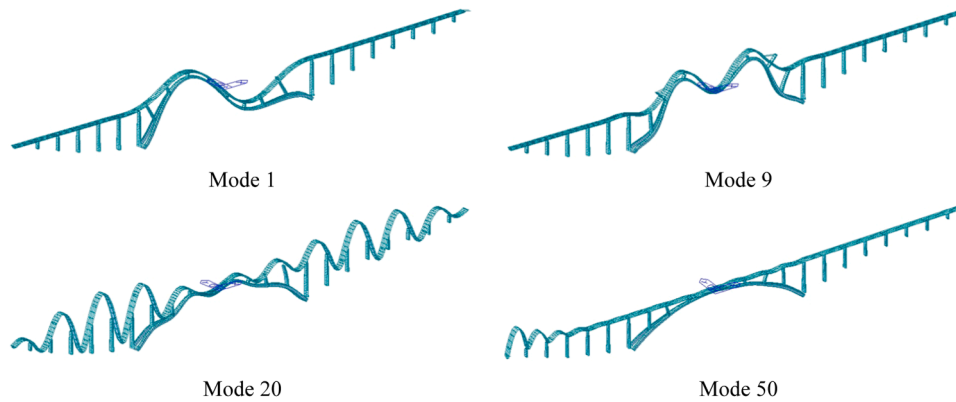


Fig. 28. Modes 1, 9, 20 and 50 of vibration of Almonte Viaduct.

respectively. Based on this analysis, zone A in Fig. 24 can be identified as the resonance zone for $n = 1$ and zone B as the resonance zone for $n = 2$. In conclusion, for the Viaduct over the Aragón River, the simplified method predicts perfectly the resonance velocities of each train that will produce acceleration amplification and also correctly predicts the points that need to be checked because it identifies the mode that will be activated.

4.2. Almonte viaduct

Case C6 is analysed below. This case is an analysis of a real bridge, the Almonte Viaduct, the world's longest high-velocity train arch bridge. Analogously to the Viaduct over the Aragón River, a dynamic analysis was carried out in the Almonte Viaduct according to Eurocode [1]. The main characteristics of the analysis are shown in Table 6. The sections analysed were the centres of spans 1, 3, 6, 7, 8, 9, 10 and 11 (centre of the bridge), Fig. 3. Spans 2 and 4 have not been considered for analysis because they have the same length as span 3, which is the typical span for approaching the arch. The simplified method for detecting resonant effects shown in the article for this real case is applied. A total of 100 modes of vibration were considered in the analysis (Table 5). Every

single mode of vibration has its corresponding resonance velocity for each type of train (different distances between axles). Some resonance velocities will be greater than the maximum velocity of the project (420 km/h), thus their main submultiples within the project's velocity range must be considered. In total, there would be 1000 velocities and 100 sections to analyse. However, by studying the shape of the modes of vibration and according to the concepts shown in this article, the number of velocities to be analysed can be reduced by discarding the modes that will not be activated significantly. To give an example of how this is done, the specific analysis of modes 1, 9, 20 and 50 is shown, Fig. 28.

The activation of mode 1 will not be significant because it goes up and down in equal parts approximately, thus the equivalent forces produced after trains A1-A10 will be cancelled, just as happened with mode 1 for cases C2 and C3. Mode of vibration 9 has the displacement in the same upward direction, so there will be a significant equivalent force. However, the length of the wave over the arch produces a minimum value of parameter $L_m/D > 3$, so the activation of mode 9 will be practically negligible. The activation of mode 20 will be residual for the same reason as that of mode 1, the spans that go up and down cancel each other's equivalent force. Actually, these arguments could be

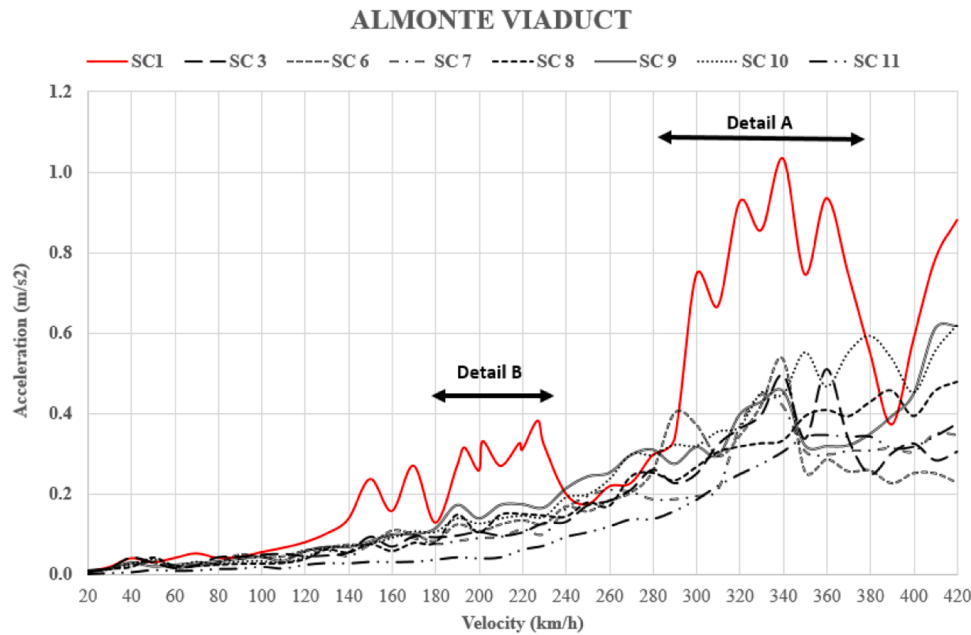


Fig. 29. Acc. Envelope. Trains A1 to A10 in SC1, SC3, SC6, SC7, SC8, SC9, SC10 and SC11. FEM.results.

Table 10

Resonance velocities of mode 50 for $n = 1$ and $n = 2$ in Almonte Viaduct.

Mode 50	$f \text{ (Hz)} = 4.67$	$V_{rm50n} \text{ (km/h)}$	
Train	D (m)	n=1	n=2
A1	18	302.7	151.4
A2	19	319.5	159.8
A3	20	336.3	168.2
A4	21	353.2	176.6
A5	22	370.0	185.0
A6	23	386.8	193.4
A7	24	403.6	201.8
A8	25	420.4	210.2
A9	26	437.2	218.6
A10	27	454.1	227.0

applied to the first 49 vibration modes of the Almonte Viaduct. However, mode 50 is the first mode that has an important equivalent force and L_m/D parameter between 1.3 and 2 depending on the train considered. For this reason, mode of vibration 50 will be activated with greater intensity. Due to the fact that mode 50 has maximum displacement at approximately the centre of span 1, this section will be the one that presents the highest accelerations. The activation of modes from 51 to 100 will be residual for the same reason as the first 49 modes. That means only the resonance velocity of mode 50 really needs to be checked.

The result of the dynamic analysis of the Almonte Viaduct that includes 100 modes of vibration for all the span centres defined in Fig. 3 is shown in Fig. 29. Each line represents the acceleration envelope of the trains A1-A10 for the corresponding check section. As can be seen, it is span 1 that develops the envelope with the highest accelerations, consistent with the activation of mode 50. Two zones of maximum accelerations in the SC1 envelope can be identified in Fig. 29, detail A and detail B.

Note that it is the centre of span 1 that presents higher accelerations, as was expected after applying the simplified method. Section SC1 was studied in detail in order to check whether the acceleration peaks are

produced due to the velocities calculated in Table 10 in the detail A and detail B zones (see Fig. 29). Here the resonance velocities ($n = 1$) of mode of vibration 50 for trains A1-A10 and the main submultiples ($n = 2$) are shown. Note that values beyond the project's range are marked in grey.

The results of the detail A zone are shown in Fig. 30. The velocities in Table 10 are highlighted by the corresponding vertical lines. As can be checked, the maximum accelerations for each train form the SC1 envelope in the range of 270 km/h to 390 km/h. Note that the maximum accelerations from dynamic analysis match with the corresponding vertical lines strongly.

The detail B zone is shown in Fig. 31 where the velocities in Table 10 for $n = 2$ and trains A6 to A10 are highlighted with vertical lines. The maximum accelerations of each train form the envelope of SC1 for velocities from 180 km/h to 250 km/h. It can be seen that the acceleration peaks match perfectly with the velocities predicted by the simplified method for each train. Below 140 km/h, the submultiples of $n > 2$ generate the envelope but, due to the damping, the peaks of accelerations remained practically eliminated, Fig. 29.

In conclusion, the simplified method also perfectly predicts, for a bridge like the Almonte Viaduct, the resonance velocities that each train

SC 1 ENVELOPE - FE MODEL RESULTS Vs. SIMP. METHOD-ALMONTE VIADUCT - Detail A

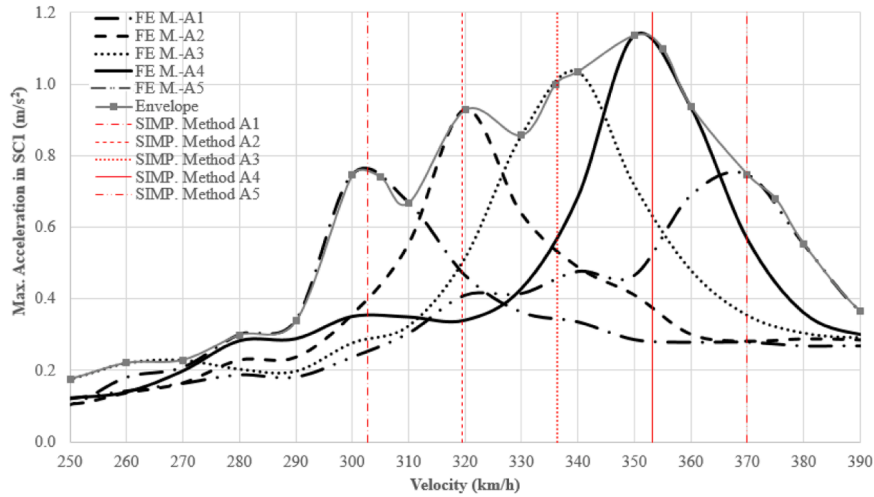


Fig. 30. Analysis of Detail A. FE model results Vs Simp. Method. Max. acc. Vs Vel. of trains (A1-A5).

SC 1 ENVELOPE - FE MODEL RESULTS Vs. SIMP. METHOD-ALMONTE VIADUCT - Detail B

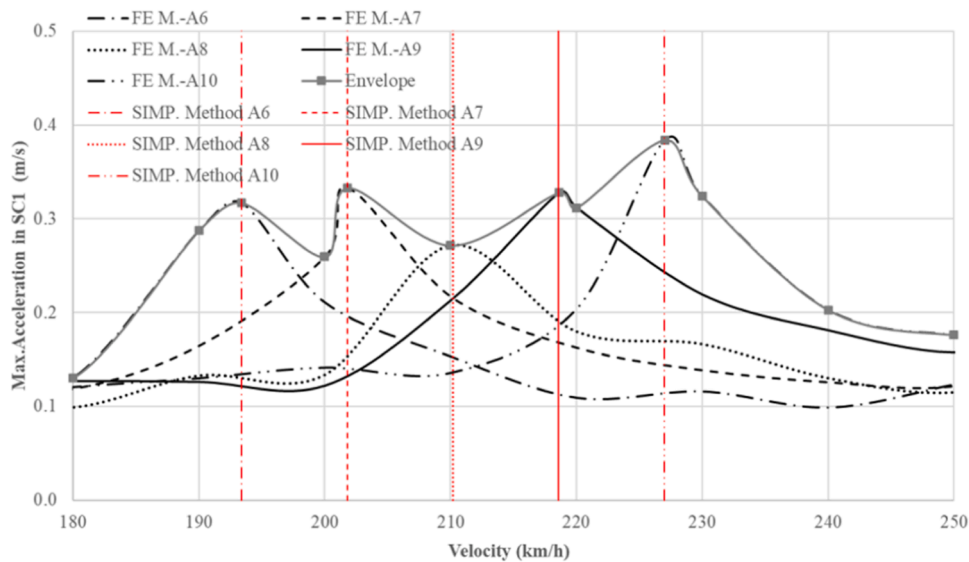


Fig. 31. Analysis of Detail B. FE Model results Vs. Simp. Method. Max. acc. Vs Vel. of trains (A6-A10).

will produce depending on the distance between axes. Additionally, the simplified method also correctly predicts the section that needs to be checked, as it identifies the main mode that will activate (mode 50) and those that will not among the 100 modes involved in the dynamic analysis.

5. Conclusions

The article presented a simplified method to calculate the sections to check and the resonance velocities that can occur in bridges. The simplified method was verified based on FE Model results in 4 ideal simple bridges and subsequently in two real High-Speed bridges of different typology. In all cases, the simplified method predicted the resonant effects and the sections of the bridge where they occur very precisely.

The main contributions and novelties of the method regarding the

existing methods are the following:

Firstly, it is the only method that enables the calculation of resonance velocity in complex bridges easily. Unlike cases of single or double-span beams discussed in the literature, the article analyses not only simple cases but also a deck arch bridge and a continuous variable-depth box girder bridge to demonstrate its validity across various typologies without increasing the difficulty. Secondly, its calculation simplicity stands out, making it faster and more manageable than other methods, providing greater practical applicability. Thirdly, it is the only method that, for each specific resonance velocity, identifies the point on the bridge where the maximum acceleration will occur by associating the resonance velocity with the excitation of a specific vibration mode. This feature is crucial when a finite element analysis is performed to detect resonance in bridges, as engineers have to decide, based on their judgment, which points along the bridge are the most critical to check for acceleration. These properties of the simplified method are based on

three novel theoretical concepts related to dynamic calculation: dynamic influence line, equivalent force, and relative span length. To use the simplified method effectively, a deep understanding of these concepts is required, which balances out its straightforward mathematical application. Finally, due to its simplicity, it is a very useful tool to easily check whether the acceleration peaks that may result from an FE model are correct or may be due to an error in the numerical modelling.

CRedit authorship contribution statement

Sánchez-Haro Javier: Writing – original draft, Methodology, Investigation, Formal analysis, Data curation, Conceptualization. **Merino Emilio:** Validation, Software, Resources, Project administration. **Capellán Guillermo:** Validation, Supervision, Resources, Funding acquisition. **Fernández Begona:** Writing – review & editing, Software, Data curation.

Declaration of Competing Interest

The authors declare that they have no known competing financial interests or personal relationships that could have appeared to influence the work reported in this paper.

Data availability

Data will be made available on request.

Acknowledgements

The authors would like to thank the company Arenas&Asociados for providing the real calculation models of the Viaduct over the Aragón River and the Almonte Viaduct. Thanks to this, both the acceleration versus velocity diagrams and the modes of vibration that were used for the design of both bridges were used in this research.

References

- [1] Eurocode 1-Actions on Structures Part 2-Traffic Loads on Bridges, 2003.
- [2] American Railway Engineering and Maintenance-of-Way Association, 2012.
- [3] Spanish Regulation. Actions considered in railway bridges (IAPF-11), 2012.
- [4] California High-speed Rail Authority. Design Criteria Manual Book III part A.1, 2015.
- [5] Sánchez-Haro J, Lombillo I, Capellán G. Modelling criteria proposal for dynamic analysis of beam bridges under moving loads using fem models. *Strucures* 2023;50: 651–69.
- [6] Yang Y-B, Yau J-D, Hsu L-C. Vibration of simple beams due to trains moving at high speeds. *Eng Struct* 1997;19(11):936–44. [https://doi.org/10.1016/S0141-0296\(97\)00001-1](https://doi.org/10.1016/S0141-0296(97)00001-1).
- [7] Li A, Su M. The resonant vibration for a simply supported girder bridge under high-speed trains. " J Sound 1999;Vibr. 224(5):897–915. <https://doi.org/10.1006/jsvi.1999.2226>.
- [8] A. Domenech P. Museros. J. Nasarre A. Castillo-Linares " Behavior of simply supported high-speed railway bridges at resonance: Analysis of the influence of the vehicle model and simplified methods for dynamic analyses" International Conference on Noise and Vibration Engineering 2 1057–1072 2012. ISBN: 978–162276825-7.
- [9] Xia H, Zhang N, Guo W. Fundamental Theories and Analytical Methods for Vibrations of Simply-Supported Beams Under Moving Loads", Book. *Adv High-Speed Rail Technol* 2017:85–147.
- [10] J.D.-Yau L. Fryba" Interaction dynamics of a high-speed train moving on multi-span railway bridges with support settlements" Proceedings of ISMA - International Conference on Noise and Vibration Engineering and USD - International Conference on Uncertainty in Structural Dynamics 995–963. 2014.
- [11] Ülker-Kaustell M, Karoumi R, Pacoste C. Simplified analysis of the dynamic soil-structure interaction of a portal frame railway bridge. *Eng Struct* 2010;32(11): 3692–8. <https://doi.org/10.1016/j.engstruct.2010.08.013>.
- [12] Liu L, Zuo Z, Yau JD, Urushadze S. A simplified method to assess vehicle–bridge interaction for train-induced vibration of light-weight railway bridges. *J Chin Inst Eng Trans Chin Inst Eng A* 2022;45(8):651–60. <https://doi.org/10.1080/02533839.2022.2126400>.
- [13] Cheng Z, Zhang N, Sun Q, Shen Z, Liu X. Research on Simplified Calculation Method of Coupled Vibration of Vehicle-Bridge System". *Shock Vibr* 2021; 9929470. <https://doi.org/10.1155/2021/9929470>.
- [14] Zhai W, Han Z, Chen Z, Ling L, Zhu S. Train–track–bridge dynamic interaction: a state-of-the-art review. " I J Veh Mech Mobil 2019;57(7). <https://doi.org/10.1080/00423114.2019.1605085>.
- [15] Xia H, Li HL, Cuo WW, De Roeck G. "Vibration Resonance and Cancellation of Simply Supported Bridges under Moving Train Loads" J. of Eng. Mechanics 2013; 140(5). [https://doi.org/10.1061/\(ASCE\)EM.1943-7889.000071](https://doi.org/10.1061/(ASCE)EM.1943-7889.000071).
- [16] Museros P, Moline E, Martínez-Rodrigo MD. Free vibrations of simply-supported beam bridges under moving loads: Maximum resonance, cancellation and resonant vertical acceleration. " J Sound Vib 2013;332(2):326–45. <https://doi.org/10.1016/j.jsv.2012.08.008>.
- [17] Yang YB, Yau JD. Resonance of high-speed trains moving over a series of simple or continuous beams with non-ballasted tracks. *Eng Struct* 2017;143:293–305. <https://doi.org/10.1016/j.engstruct.2017.04.022>.
- [18] Martínez-Rodrigo MD, Andersson A, Pacoste C, Karoumi R. Resonance and cancellation phenomena in two-span continuous beams and its application to railway bridges. *Eng Struct* 2020;222(1). <https://doi.org/10.1016/j.engstruct.2020.111103>.
- [19] H. Bigelow B. Hoffmeister and M. Feldmann " Simplified design of filler beam railway bridges for high-speed traffic" Proceedings of ISMA - International Conference on Noise and Vibration Engineering and USD 2018 - International Conference on Uncertainty in Structural Dynamic. 1621–1934 2018. ISBN: 978–907380299-5.
- [20] Jesus AH, Dimitrová Z, Silva MAG. A statistical analysis of the dynamic response of a railway viaduct. *Eng Struct* 2014;71:224–59. <https://doi.org/10.1016/j.engstruct.2014.04.012>.
- [21] Xin L, Mu D, Choi D-H, Li X, Wang F. General conditions for the resonance and cancellation of railway. *Mech Syst Signal Process* 2023;183:109589. <https://doi.org/10.1016/j.msssp.2022.109589>.
- [22] Wang S, Zhao W, Zhang G, Li F, Du Y. Fourier Series Approach for the Vibration of Euler–Bernoulli Beam under Moving Distributed Force: Application to Train Gust. *Shock Vib* 2019;2542349. <https://doi.org/10.1155/2019/2542349>.
- [23] Yang X, Yi T, Qu C, Li H, H, Liu H. Performance Warning of Bridges under Train Actions through Equivalent Frequency Response Functions. *J Bridge Eng* 2022;7 (10). [https://doi.org/10.1061/\(ASCE\)BE.1943-5592.0001925](https://doi.org/10.1061/(ASCE)BE.1943-5592.0001925).
- [24] Ding Y, Zhao H, Deng L, Li A, Wang M. Early warning of abnormal train-induced vibrations for a steel-truss arch railway bridge: case study. *J Bridge Eng* 2017;22 (11). [https://doi.org/10.1061/\(ASCE\)BE.1943-5592.0001143](https://doi.org/10.1061/(ASCE)BE.1943-5592.0001143).
- [25] Yhang X, Yi T, Qu C, Li H, Liu H. Modal Identification of High-Speed Railway Bridges through Free-Vibration Detection. " J Bridge Eng 2020;146(9). [https://doi.org/10.1061/\(ASCE\)EM.1943-7889.0001847](https://doi.org/10.1061/(ASCE)EM.1943-7889.0001847).
- [26] Gattulli V, Lofrano E, Paolone A, Potenza F. Measured properties of structural damping in railway bridges. " J Civ Stru Health M 2019;9:639–53. <https://doi.org/10.1007/s13349-019-00358-3>.
- [27] Khodabandehlou H, Pekcan G, Fadall MS. Vibration-based structural condition assessment using convolution neural networks. *Struct Control H Monit* 2018;26(2). <https://doi.org/10.1002/stc.2308>.
- [28] Nguyen DC, Salamat M, Katunin A, Gerges M. Finite Element Model Updating of RC Bridge Structure with Static Load Testing: A Case Study of Vietnamese ThiThach Bridge in Coastal and Marine Environment. *J Sens* 2022;22(22):8884. <https://doi.org/10.3390/s22228884>.
- [29] Hakim S, Konstantinovich D. "Study of dynamic impact of speed trains on bridge structures. *Int J Mech* 2021;15:30–6. <https://doi.org/10.46300/9104.2021.15.4>.
- [30] Grebowski K, Zielińska M. Dynamic analysis of historic railway bridges in Poland in the context of adjusting them to Pendolino trains. *Int J Appl Mech* 2015;20 (2):283–97. <https://doi.org/10.1515/ijame-2015-0019>.
- [31] Zeying Y, Chenghe W, Zhilin Q, Rongrong D, Yinglin S, Feng Z. Static and Dynamic Behavior of the High-Pier and Long-Span Continuous Rigid Frame Bridge. *Adv Mater Res* 2013;639-640:474–80. <https://doi.org/10.4028/www.scientific.net/AMR.639-640.474>.
- [32] Hao L, Chuyi X, Xianbei G, Moungun L, Xiangrong G, Hui G. The Train-Bridge Coupled Vibration Analysis of a Long-Span Prestressed Concrete Continuous Beam Bridge under Creep Deformation Effect. *J Appl Sci* 2022;12(22):11838. <https://doi.org/10.3390/app122211838>.
- [33] Ahmed F, Khaled E, Hany A. Seismic performance of cable-stayed bridges with different geometric conditions. *J Eng Appl Sci* 2022;69:82. <https://doi.org/10.1186/s44147-022-00115-2>.
- [34] Rafiee-Dekhkharghani R. Ghyasvand S. Sahebzalmani P. "Dynamic Behavior of Masonry Arch Bridge under High-Speed Train Loading: Veresk Bridge Case Study" Journal of Performance of Constructed Facilities32(3) 040180162018; 10.1061/(ASCE)CF.1943-5509.0001158.
- [35] Zhao H.W. Ding Y.L. An Y.H. Li A.Q. "Transverse Dynamic Mechanical Behavior of Hangers in the Rigid Tied-Arch Bridge under Train Loads" Journal of Performance of Constructed Facilities31(1) 040160722017; 10.1061/(ASCE)CF.1943-5509.0000932.
- [36] Póvoas A.A. "Building the decks of the world's largest high speed train arch bridges with movable scaffolding systems" Multi-Span Large Bridges - Proceedings of the International Conference on Multi-Span Large Bridges615–6232015; 10.1201/b18567-79.
- [37] Reina P. "World's longest arch bridge for high-speed rail takes shape" *ENR (Engineering News-Record)*275(6) 2016; ISBN: 8919526.
- [38] Capellán G. Merino E. Sacristán M. Guerra S. García P. "Almonte Viaduct: Design Principles and Structural Monitoring" *Structural Integrity*11706–7142020; 10.1007/978-3-030-29227-0_77.

- [39] Capellán G, Merino E, Sacristán M, Martínez J, Guerra S. "Recent developments in concrete arch bridges" *fib Symposium* 112621–26282018; 10.1007/978–3–319–59471–2_298.
- [40] Arenas J.J, Capellán G, Martínez-Aparicio J, Guil Y, García-Arias P. "Viaduct over river almonte. Design and analysis" *IABSE Congress Stockholm: Challenges in Design and Construction of an Innovative and Sustainable Built Environment* 2345–23522016; ISBN: 978–385748144-4.
- [41] Arenas JJ, Merino E, García P, Beade H, Guil Y. "Analysis and design of the Almonte Bridge". *Eng Prog Nat People* 56 2014;63. <https://doi.org/10.2749/222137814814027431>.